

***In Toto* Adipocytes Analysis using Hydrophilic Tissue Clearing, LightSheet Microscopy, and Deep Learning-Based Image Processing**

Running title: *In Toto* Adipocytes Analysis via Clearing & LSM

Dylan Le Jan ¹, Manar Harb ², Mohamed Siliman Misha ¹, Jean-Claude Desfontis ¹, Yassine Mallem ^{1,*}, Laurence Dubreil ^{2,*}

1: Oniris, NP3 (Nutrition, PathoPhysiology & Pharmacology), 44307, Nantes, France;

2: Oniris, INRAE, APEX PAnTher, 44307, Nantes, France.

* Corresponding authors: laurence.dubreil@oniris-nantes.fr, yassine.mallem@oniris-nantes.fr

ABSTRACT

Background information: Obesity is a multifactorial metabolic disease characterized by excessive fat storage in adipocytes, particularly in visceral adipose tissue like mesenteric adipocytes. Metabolic dysfunctions due to obesity is often associated to modification of adipocytes volume. Various techniques for measuring adipocyte size are described in the literature, including classical histological methods on paraffin-embedded tissue sections or dissociation of adipose tissue using collagenase with artifacts due to adipose tissue post treatment.

Results: This study aims to develop and implement an innovative method for 3D investigation of adipose tissue to assess adipocyte volume, overcoming the limitations and biases inherent in traditional techniques. The principle of the method relies on fluorescent labeling of lipids and extracellular matrix *in toto* within adipose tissue, followed by a tissue clearing step without delipidation and imaging using 3D LightSheet microscopy coupled with automated analysis of adipocyte size through a deep learning approach. By this work we showed that volume of adipocytes increased in mesenteric adipose tissue from obese rats with an increase in the distance between adipocytes.

Conclusion and significance: The current work highlights the interest to combine adipose tissue clearing without delipidation step and LightSheet microscopy for *in toto* 3D adipocyte characterization in obese *versus* healthy rats. While this method is particularly valuable for understanding adipocyte hypertrophy in the context of obesity, its applicability extends beyond this area. This innovative approach offers valuable opportunities to investigate adipocyte dynamics in various pathological conditions, evaluating the impact of nutritional interventions, and assessing the effectiveness of pharmacological treatments.

KEYWORDS

Mesenteric adipose tissue; Tissue clearing; LightSheet microscopy; Adipocyte volume; Image analysis

ABBREVIATIONS

5-DTAF (5-(4,6-dichlorotriazinyl)aminofluorescein); AT (adipose tissue); ECM (extracellular matrix); GA3 (general analysis 3); HFD (high-fat diet); NOD (nearest object distance); RI (refractive index); VAT (visceral adipose tissue)

INTRODUCTION

Obesity is a complex metabolic disorder influenced by various factors, including environmental conditions, diet, and genetics (Hruby and Hu, 2015). The central mechanism underlying obesity is an imbalance between caloric intake and energy expenditure, leading to excess fat storage, primarily in adipocytes located in visceral adipose tissue (VAT), such as mesenteric adipocytes (Ali et al., 2013; Frayn, 1993). Hypertrophy of these adipocytes, often accompanied by hypoxia, leads to systemic inflammation and insulin resistance, both of which are key contributors to obesity-related metabolic complications (Chan and Hsieh, 2017).

The evaluation of adipocyte size is a crucial indicator of structural changes associated with obesity (Theobalt et al., 2021). An increased adipocyte volume has been identified as a predictive factor for the higher risk of obesity-related type 2 diabetes, with specific volume thresholds correlating with greater insulin resistance (Cotillard et al., 2014). Several techniques for measuring adipocyte size are described in the literature, including classic histological methods on paraffin-embedded tissue sections, dissociation of adipose tissue using collagenase to measure the size of isolated adipocytes (Björnheden et al., 2004), as well as flow cytometry, which also represents a useful tool for evaluating adipocyte volume (Hagberg et al., 2018).

2D approaches, which focus on parameters like cell diameter or surface area, although useful for basic analyses, do not provide reliable measurements of adipocyte volume (Laforest et al., 2015). Indeed, traditional 2D methods are prone to operator-dependent errors and require labor-intensive manual analysis (Chen and Farese, 2002). This is illustrated by 2D studies showing that the equivalent diameter index can reveal up to 23% uncertainty in glioma size due to variations in scanning conditions (Schmitt et al., 2013). Furthermore, the analysis of

adipocyte size on thin histological paraffin sections requires a tissue delipidation step, which can alter adipocyte structure and prevent access to cellular volume. Additionally, dissociating tissue with collagenase allows adipocytes to be freed from the tissue but also releases stromal/vascular cells that can contaminate the samples and bias the results (Majka et al., 2014). This limitation is particularly relevant in flow cytometry, where the presence of non-adipocyte cells can interfere with gating strategies and affect the accuracy of adipocyte volume estimation. Moreover, the large size and fragility of adipocytes make them prone to deformation or rupture during flow-based measurements, further limiting the reliability of this approach. Furthermore, 3D imaging of adipocytes is limited to a few tens of micrometers in confocal microscopy (Blackshear et al., 2018), due to the opacity of adipose tissue, which causes light scattering. Indeed, the heterogeneous composition of tissues (lipids, carbohydrates, proteins, colored pigments bathed in interstitial fluids) results in a variety of refractive indices (RI) responsible for light scattering (Azaripour et al., 2016).

The tissue clearing technique, making tissues optically transparent, offers a promising solution and has become a powerful tool for *in toto* three-dimensional analysis (Costa et al., 2019; Costantini et al., 2019). However, these techniques are still underused in obesity research, particularly when it is important to preserve lipid storage. Indeed, current tissue clearing techniques used on adipose tissue rely on organic solvents to remove storage lipids in order to study 3D structures of the tissue such as vascularization, innervation and crownlike structures (Chi et al., 2018; Geng et al., 2021), but they do not allow the analysis of adipocytes that are altered after delipidation steps.

In this study, we propose a new 3D approach to investigate preserved whole adipocytes in cleared adipose tissue (AT). This new approach involves fluorescent staining of AT with red Nile and 5-(4,6-dichlorotriazinyl)aminofluorescein (5-DTAF) fluorescent probes for lipids and extracellular matrix (ECM), respectively. Then, fluorescent AT is cleared by immersion in a high RI solution (RapiClear®) without delipidation step and imaged by LightSheet microscopy to be analyzed by developing a workflow combining AI segmentation and deep learning tools. These techniques enable an accurate evaluation of new critical parameters on adipocyte morphology such as volume, density, and sphericity, for a more precise and comprehensive evaluation of structural changes in adipocytes associated with obesity. The consideration of

these new morphologic parameters could contribute in understanding the processes of adipocyte hypertrophy, especially in the context of obesity, and could be used to assess therapies developed to manage obesity.

MATERIALS & METHODS

Animals and tissue sample preparation

Six male Wistar rats (8 weeks old) were obtained from Janvier Labs® (Le Genest-Saint-Isle, France) and acclimatized for one week prior to the study. The animals were housed in accordance with European standard ETS 123, under a controlled 12-hour light/dark cycle, with a temperature maintained at 22 ± 2 °C and 50% relative humidity.

This study received approval from the Ethics Committee on Animal Experimentation of the Pays de la Loire Region (APAFIS#33784-2021112413036973v3, 13 December 2021), in compliance with the guidelines of the French National Research Council for the Care and Use of Laboratory Animals.

The rats were randomly divided into two groups (n=3 per group). The Healthy group was fed a standard diet (3430 Kliba Nafag, Kaiseraugst, Switzerland), while the Obese group received a high-fat diet (HFD). The HFD consisted of pellets (D12451 Research Diets®, Lynge, Denmark) and sweetened condensed milk (Nestlé®, Nantes, France), both provided *ad libitum* for 26 weeks. To ensure the proper induction of obesity through dietary intervention, no significant differences in body weight were observed between groups at the start of the study. After 26 weeks of either standard diet or HF diet, the Healthy and Obese groups exhibited mean body weights of 623.00 ± 20.03 g and 735.27 ± 12.04 g, respectively, representing an approximate difference of 18.04%. In rats, moderate obesity is typically defined as a body weight increase ranging from 10% to 25% (Bagnol et al., 2012), allowing us to categorize the HFD-fed animals as obese.

At the end of the study, the rats were euthanized by an overdose of intraperitoneal anesthetic (pentobarbital, Euthasol®, Fort Worth, TX, USA), followed immediately by the collection of mesenteric AT.

Adipose tissue staining and clearing

Mesenteric AT was collected from rats after euthanasia. For fixing, samples were stored in 4% formaldehyde for at least 72 hours. After cutting off part of the AT (around 3 mm thick), they were washed in PBS (Sigma®; 806552) 3 times, 1 hour each, with stirring (750 rpm) at room temperature. Stock solutions of Nile Red (ThermoFisher®, N1142-25mg, Waltham, MA, USA) and 5-DTAF (ThermoFisher®, 11550216, Waltham, MA, USA) were prepared at 1 mg/mL in DMSO and at 10 mg/mL in PBS, respectively, and stored in the freezer at -20°C. A mixture of Nile Red and 5-DTAF were diluted at 1/50 and 1/1000 in PBS, respectively. Samples were incubated firstly for 24 hours in Nile Red 1/50. After that, the staining medium was replaced with mixture of Nile Red + 5-DTAF and left to shake at room temperature for 24 hours. Rinsing was carried out in PBS 3 times for 2 hours each. To facilitate the handling and imaging of AT with the LightSheet, samples were embedded in 2% agarose (low melting A0701, Sigma Aldrich®, St. Louis, MO, USA) prior clearing. Agarose was dissolved in PBS and heated using a water bath of 60°C to have a liquid solution. Samples were totally covered to create a mould. Samples were then removed from mould after solidification and agarose was trimmed as close as possible to the sample before immersion in RapiClear 1.47 (RapiClear®, RC147001, SunJin Lab, Hsinchu City, Taiwan) during 2 days on a stirrer at room temperature (Figure 1). After that, RapiClear solution was change and incubate at least 24h before imaging with the control of RI value by using a refractometer (Mettler Toledo, PortableLabTM, France). This step was done to prevent modification of RI by water releasing from agarose.

LightSheet imaging

Cleared samples were images with a Blaze LightSheet microscope (Miltenyi Biotec, Bergisch Gladbach, Germany) equipped with sCMOS camera 5.5 MP controlled by Inspector Pro acquisition software (Miltenyi Biotec, Bergisch Gladbach, Germany). Images were acquired with two different lasers: the 488 nm laser was used to excite the 5-DTAF dye (for extracellular matrix staining) and the 561 nm laser was used for the excitation of the Nile Red dye (for lipid staining). The imaging was done with a 4X objective lens (NA 0.35). Samples were supported by a sample holder from Miltenyi and placed in a tank filled with mineral oil with RI 1.47 (M3516, Sigma Aldrich®, St. Louis, MO, USA) and illuminated by the laser LightSheet from both

sides. LightSheet thickness 4 μ m, step size 4 μ m. The images were acquired with a camera sCMOS, exposure time 50 ms, 2048x2048, pixel size 1.62 μ m.

Three-dimensional images analyses

LightSheet images from cleared AT were post-processed with Miltenyi software MACS to do crop 3.32mmX3.32mmX0.4mm and processed using NIS software Nikon 5.42.03 (Nikon Europe B.V., Amstelveen, The Netherlands). Due to variations in fluorescent signal intensity and the proximity of contiguous objects of interest, manual segmentation was deemed unsuitable as it introduced variability in the results. Consequently, we opted to implement a deep learning-based segmentation approach to enhance the reproducibility and efficiency of the measurements (Figure 2). Segmentation was conducted using the U-Net-based deep learning model "SegmentObject.ai," integrated into the NIS-Elements software. Deep learning training:

The training algorithm was conducted in two rounds. In the first round, the dataset consisted of three images obtained from an averaged Z-stack, with five frames per stack. The three representative planes—the first, middle, and last—were saved separately, followed by manual thresholding of the structure of interest. AT was initially identified using intensity-based thresholding, with subsequent manual refinement to generate precise binary masks. These refined masks served as the ground truth for model training, which was carried out for up to 200 iterations.

The resulting algorithm was applied to a dataset comprising 16 images extracted using the same procedure. The binary mask images generated were manually corrected and cropped to produce final images containing between 5 and 10 adipocytes. These corrected binary masks from the 16 cropped images were used as the ground truth for the second round of training, which was conducted over 1500 iterations. This process resulted in a more robust and accurate segmentation algorithm (score training curve Loss < 0.003). To verify its consistency with the previous version, the updated algorithm was applied to a cropped image as a validation step (Figure 2.A).

The resulting algorithm was subsequently imported into a General Analysis 3 (GA3) pipeline for further feature measurements (Figure 2.B). 3D images (2042.82 μ m x 1885.68 μ m x 380

μm) from 3 healthy and 3 obese rats were analyzed to assess key morphological features, including total object volume, object count, individual object volume, equivalent diameter, sphericity, and nearest object distance (NOD). The GA3 pipeline was developed to extract and quantify various features of AT from 3D images. This approach leverages deep learning-based segmentation and advanced image processing techniques to investigate the structural organization of adipose tissue. The pipeline begins with the application of U-Net-based deep learning models. Segment.Object.ai is used for segmenting red-stained adipocytes. A binary operation, "separate objects," is applied to divide connected adipocyte structures into smaller individual objects. A second binary operation, "circular open," is used to remove regions that cannot accommodate a circle or sphere of the adipocyte. Measurements are then performed, including: The number and volume of adipocytes, NOD, equivalent diameter and sphericity of the adipocyte, and the total object volume of both adipocytes and the ECM.

This 3D pipeline provides an integrated framework for characterizing the structural organization of adipose tissue in a three-dimensional context. The extracted data were subsequently exported for statistical analysis (Figure 2).

Each individual sample consisted of 450 analyzed adipocytes (n=1350 adipocytes per group). Four key parameters were assessed to evaluate the morphology of the adipocytes. The first parameter was the 3D volume of each adipocyte. The second parameter, the Nearest Object Distance (NOD), corresponded to the smallest distance to another adipocyte (measured between centers of gravity). The third parameter was the equivalent diameter, which was calculated by the software as the diameter of a sphere with the same volume as the measured adipocyte. Finally, the sphericity of each adipocyte was evaluated, which was computed as the ratio of the adipocyte surface and the surface of a sphere with matching volume. A sphere has the maximum sphericity=1.

Statistical analysis

Results are expressed as mean ± standard error of the mean (SEM). Statistical analyses were performed using GraphPad Prism® (v.9.0.0). Comparisons of means were conducted using Mann-Whitney tests, while distribution analyses were performed using multiple Mann-Whitney tests for pairwise comparisons between groups, with multiple comparisons corrected

using the false discovery rate approach at a Q value of 5%. A p-value < 0.05 was considered statistically significant.

RESULTS

3D visualization of adipocyte from Nile red staining, RapiClear clearing of adipose tissue combined with LightSheet microscopy

Lipids were stained with Nile Red, in accordance with published data (Greenspan et al., 1985), while the ECM was stained with 5-DTAF (Graham et al., 2017). The 3D structure of mesenteric adipocytes within AT was investigated using RapiClear, a clearing reagent that preserves storage lipids (Chen et al., 2021; Horckmans et al., 2022) and retaining the fluorescent labeling (Figure 1). Unlike solvent-based clearing techniques such as uDISCO (Pan et al., 2016), which typically cause tissue rigidification, AT cleared with RapiClear remained soft and flexible. To facilitate LightSheet imaging, we embedded the tissue in agarose before the clearing process.

Images were then acquired using the Ultramicroscope Blaze, equipped with a 4X objective and an immersion tank filled with mineral oil (RI 1.467), closely matching the RI 1.47 of RapiClear (Figure 1). Adipocytes as well as the ECM surrounding the adipocytes *in situ* within AT was imaged over several millimeters in surface area but the depth was limited to half millimeter. Indeed, the clearing of AT was not fully optimized, as storage lipids significantly contribute to tissue opacity (Tian et al., 2021).

A 3D reconstruction of RapiClear 1.47 cleared AT stained with Nile red (adipocyte lipids in red) and 5-DTAF (ECM in green) in both healthy and obese animal is shown in Figure 3.

Image quality was acceptable for depths up to 400 μm , which allowed for correct segmentation of objects using the segmentobject.ai algorithm developed from NIS. The segmentation process was refined through successive annotations and training cycles. The quality of the segmentation and consequently the deep learning algorithm, was validated by the loss training curve (score 0.00279; 1500 iterations) and overlay of the annotation with segmentation produced by updated algorithms (Figure 2). This analysis was performed on

Healthy and Obese groups after 26 weeks on a diet to quantify morphological characteristics and distribution patterns of adipocytes into AT.

3D new features to characterize adipocytes in tissue: Volume, Density, Diameter, Sphericity

The mean adipocyte volume was measured on 450 adipocytes of each sample (Figure 4.A). A Significant difference was observed between adipocyte volume of Obese group ($299,242 \pm 7,342 \mu\text{m}^3$) and the Healthy group ($248,754 \pm 5,129 \mu\text{m}^3$), reflecting an approximate 20.30% increase in volume with obesity ($p < 0.001$).

In addition, the mean NOD measured between adipocytes was significantly higher in the Obese group ($66.23 \pm 0.64 \mu\text{m}$) compared to the Healthy group ($61.91 \pm 0.43 \mu\text{m}$), representing a 6.98% increase ($p < 0.001$) (Figure 4.B).

In contrast, the mean equivalent diameter, did not show a statistically significant difference between the groups. The Obese group had a mean equivalent diameter of $72.13 \pm 0.76 \mu\text{m}$, while the Healthy group measured $71.17 \pm 0.58 \mu\text{m}$ (Figure 4.C).

Similarly, mean sphericity remained relatively stable between conditions, with the Obese group displaying a mean value of 0.813 ± 0.002 and the Healthy group at 0.820 ± 0.002 , indicating a difference of less than 1% (Figure 4.D).

3D features distribution provides additional insights to characterize adipose tissue

The distribution of adipocyte volume exhibited distinct patterns between the two diet groups. In the Healthy group, adipocytes were predominantly found in moderate volume categories ($100,000\text{--}300,000 \mu\text{m}^3$), whereas the Obese group contained a higher number of adipocytes in larger volume classes, particularly those exceeding $500,000 \mu\text{m}^3$ (Figure 5.A).

Similarly, NOD distribution varied between groups. In the Healthy group, adipocytes were most prevalent in medium-distance categories ($50\text{--}70 \mu\text{m}$), while the Obese group displayed a greater frequency in higher NOD values. A peak was observed in the $60\text{--}65 \mu\text{m}$ range for the Healthy group, whereas the Obese group peaked in the $70\text{--}75 \mu\text{m}$ range (Figure 5.B).

For equivalent diameter, the Obese group showed a larger proportion of adipocytes in higher diameter classes ($>100 \mu\text{m}$), while the Healthy group had more adipocytes in moderate ranges

(60–90 μm). The distribution peaked at 70–80 μm for the Healthy group and 80–90 μm for the Obese group (Figure 5.C).

Finally, the distribution of sphericity appeared comparable between the two groups. The Healthy group showed a slight predominance in higher sphericity categories, while the Obese group had a greater frequency in medium sphericity ranges, particularly within the 0.76–0.88 range (Figure 5.D).

DISCUSSION

The aim of this study was to develop a method for the 3D analysis of adipocyte morphological characteristics in mesenteric AT from both obese and healthy rats while preserving adipocyte integrity. VAT was specifically chosen due to its central role in metabolic dysfunctions associated with obesity, particularly those induced by an obesogenic diet. In rats, different anatomical regions are prone to fat accumulation, including epididymal, perirenal, and mesenteric fat depots (Tchkonia et al., 2013).

Unlike subcutaneous adipose tissue, VAT is metabolically more active and plays a critical role in systemic inflammation regulation, insulin resistance, and lipid metabolism alteration (Hajer et al., 2008). VAT is also a key producer of adipokines and modulates the inflammatory environment through macrophage-derived pro-inflammatory cytokines, such as IL-6 and TNF- α , which are elevated in obesity and contribute to chronic low-grade inflammation (Balistreri et al., 2010). Mesenteric adipose tissue, located around the intestines, is particularly relevant as it plays a crucial role in local and systemic inflammation, it directly impact metabolic diseases such as insulin resistance, and is tightly connected to the intestinal barrier and microbiota (Kredel and Siegmund, 2014). These characteristics make it a critical site for evaluating the effects of an obesogenic diet on obesity progression.

3D exploration of adipose tissue through microscopy requires optical clearing techniques to reduce light scattering. A major challenge was clearing the tissue while preserving adipocyte structures, as most clearing techniques involve a delipidation step to remove the lipids mainly responsible of the tissue opacity. Our gentle clearing method, based on simple immersion in a high-refractive-index solution (RapiClear), successfully preserved lipids, minimized tissue

deformation, and preserves fluorescence staining (Gomariz et al., 2018; Lallemand et al., 2020).

Many organic solvents used for tissue clearing cause a substantial dehydration and, thus, tissue shrinkage, as well as the quenching of fluorescent staining or fluorescent protein emission (Tian et al., 2021). Notably, RapiClear is compatible with preserving endogenous fluorescent proteins such as GFP and YFP (Aihara et al., 2020; Stefaniuk et al., 2016), enhancing the versatility of our method. These fluorescent proteins are widely used for studying metabolic disorders, inflammation in AT (Neugebauer et al., 2024), adipocyte progenitor differentiation (Girousse et al., 2019), and monitoring of the AT browning process (Chan et al., 2018), providing insights into metabolic adaptations and therapeutic strategies for obesity.

Using RapiClear immersion, adipose tissue imaging in our study was limited to 400 μm in depth. However, this limitation was offset by the ability to perform rapid imaging of large samples thanks to LightSheet microscopy (Ryu et al., 2023). This approach is particularly suitable for studying large-scale AT architecture while maintaining high-resolution structural details. Furthermore, the cost-effectiveness of mineral oil with a refractive index of 1.47, used as an imaging medium in the LightSheet tank, offers a financially viable alternative for large-scale or repeated studies.

Our findings align with existing literature, although 3D studies on adipocyte volume remain scarce. For instance, studies on mice fed a HFD for 11 weeks reported increased adipocyte surface area in gonadal AT (LeMieux et al., 2015). Similarly, Ramírez et al. (2017) observed a higher area and equivalent diameter in visceral adipocytes of rats subjected to an HFD for 8 weeks. Jing et al. (2021) reported that adipocytes in rats on a 6-week HFD were engorged with fat, with significantly larger equivalent diameters, perimeters, and areas.

While these studies consistently highlight adipocyte size enlargement, our results indicate that adipocyte volume is a more relevant parameter than equivalent diameter in our model. Unlike 2D measurements, 3D imaging captures the full spatial dimensions of adipocytes, enabling more comprehensive characterization of AT. 3D analysis revealed NOD as a new discriminant parameter between Obese and Healthy animals with an increase of the distance between nearest adipocytes in Obese samples. This NOD increase may indicate tissue disorganization

and be linked to pathological ECM accumulation, particularly collagen, within Obese AT (Ruiz-Ojeda et al., 2019). As adipocytes enlarge, excessive ECM buildup may restrict adipocyte expansion, impair angiogenesis, and exacerbate local inflammation and metabolic dysfunctions (Sun et al., 2011). In the context of obesity, AT inflammation marked by macrophage accumulation around dying adipocytes in ‘crown-like structures’ disrupts tissue architecture. Macrophage infiltration and adipocyte necrosis compromise cellular integrity, potentially explaining the observed increase in NOD. These processes alter the spatial proximity between cells, further affecting the overall structure of the AT (Marcelin et al., 2022). These findings highlight the importance of 3D analysis for a more precise understanding of adipose tissue remodeling in obesity.

Our method also has significant potential for monitoring the effectiveness of nutritional interventions, such as vitamin D and omega-3 supplementation, in obesity management (Le Jan et al., 2024) as well as strategies to mitigate adipose tissue aging (Wang et al., 2022). Additionally, it may be useful in assessing the impact of pharmacological treatments, particularly GLP-1 receptor agonists, in promoting weight loss and metabolic improvements (Singh et al., 2022). Beyond obesity, this approach could be applied to study adipocyte morphological changes in pathological contexts, such as pericardial AT remodeling in myocardial infarction (Horckmans et al., 2018) or adipocyte function alterations associated with anorexia nervosa (Xiao et al., 2020).

In conclusion, the 3D analysis of AT using tissue clearing without a delipidation step, combined with LightSheet microscopy for whole-sample adipocyte characterization, presents a promising approach for comparing adipocyte morphology in obese *versus* healthy rats. By refining adipocyte imaging and 3D quantification, our method leads the way for more accurate and comprehensive studies on AT dynamics. This advancement not only deepens our understanding of adipocyte-driven pathophysiology but also provides a powerful tool for developing and evaluating therapeutic strategies targeting metabolic diseases.

ACKNOWLEDGEMENTS

We thank the staff of the APEX platform (INRAE/Oniris, Center of Excellence Nikon Nantes [CENN], Nantes, France) at UMR 0703 PAnTher (INRAE/Oniris, Nantes, France) for

technological support. We sincerely thank Ibrahim Hassani, PhD student at UMR703 in collaboration with Nikon France Healthcare, succursale Nikon Europe BV, for his assistance in implementing the pipeline GA3 from Nikon Imaging Software used in this study. The authors also thank Biogenouest (the western French network of technology core facilities in life sciences and the environment, supported by the Conseil Régional des Pays de la Loire), as well as the NeurAtris Infrastructure for supporting APEX. We extend our appreciation to SunJinLab for valuable assistance with the clearing process, and insightful technical guidance. We also thank the students who participated to the image annotation for this work (Solène Morice, Arthur Boscher).

AUTHOR CONTRIBUTIONS

Dylan Le Jan: Conceptualization, Analysis, Methodology, Writing, Review & Editing. Manar Harb: Methodology, Pipeline image analysis, Analysis, Writing, Review & Editing. Mohamed Siliman Misha: Review & Editing. Jean-Claude Desfontis: Supervision, Review & Editing. Yassine Mallem: Project Administration, Supervision, Review & Editing. Laurence Dubreil: Conceptualization, Methodology, image analysis, Supervision, Validation, Writing, Review & Editing.

CONFLICT OF INTEREST STATEMENT

The authors declare no conflicts of interest.

REFERENCES

- Ali, A.T., Hochfeld, W.E., Myburgh, R., Pepper, M.S., 2013. Adipocyte and adipogenesis. *European Journal of Cell Biology* 92, 229–236. <https://doi.org/10.1016/j.ejcb.2013.06.001>
- Azaripour, A., Lagerweij, T., Scharfbillig, C., Jadcak, A.E., Willershausen, B., Van Noorden, C.J.F., 2016. A survey of clearing techniques for 3D imaging of tissues with special reference to connective tissue. *Progress in Histochemistry and Cytochemistry* 51, 9–23. <https://doi.org/10.1016/j.proghi.2016.04.001>
- Bagnol, D., Al-Shamma, H.A., Behan, D., Whelan, K., Grottick, A.J., 2012. Diet-Induced Models of Obesity (DIO) in Rodents. *Current Protocols in Neuroscience* 59, 9.38.1–9.38.13. <https://doi.org/10.1002/0471142301.ns0938s59>
- Balistreri, C.R., Caruso, C., Candore, G., 2010. The Role of Adipose Tissue and Adipokines in Obesity-Related Inflammatory Diseases. *Mediators of Inflammation* 2010, 802078. <https://doi.org/10.1155/2010/802078>

- Björnheden, T., Jakubowicz, B., Levin, M., Odén, B., Edén, S., Sjöström, L., Lönn, M., 2004. Computerized Determination of Adipocyte Size. *Obesity Research* 12, 95–105. <https://doi.org/10.1038/oby.2004.13>
- Blackshear, C.P., Borrelli, M.R., Shen, E.Z., Ransom, R.C., Chung, N.N., Vistnes, S.M., Irizarry, D., Nazerali, R., Momeni, A., Longaker, M.T., Wan, D.C., 2018. Utilizing Confocal Microscopy to Characterize Human and Mouse Adipose Tissue. *Tissue Engineering Part C: Methods* 24, 566–577. <https://doi.org/10.1089/ten.tec.2018.0154>
- Chan, P.-C., Hsieh, P.-S., 2017. The Role of Adipocyte Hypertrophy and Hypoxia in the Development of Obesity-Associated Adipose Tissue Inflammation and Insulin Resistance, in: Gordeladze, J.O. (Ed.), *Adiposity - Omics and Molecular Understanding*. InTech. <https://doi.org/10.5772/65458>
- Chan, X.H.D., Balasundaram, G., Attia, A.B.E., Goggi, J.L., Ramasamy, B., Han, W., Olivo, M., Sugii, S., 2018. Multimodal imaging approach to monitor browning of adipose tissue in vivo [S]. *Journal of Lipid Research* 59, 1071–1078. <https://doi.org/10.1194/jlr.D083410>
- Chen, H.C., Farese, R.V., 2002. Determination of adipocyte size by computer image analysis. *Journal of Lipid Research* 43, 986–989. [https://doi.org/10.1016/S0022-2275\(20\)30474-0](https://doi.org/10.1016/S0022-2275(20)30474-0)
- Chen, Q., Lai, S.M., Xu, S., Tan, Y., Leong, K., Liu, D., Tan, J.C., Naik, R.R., Barron, A.M., Adav, S.S., Chen, J., Chong, S.Z., Ng, L.G., Ruedl, C., 2021. Resident macrophages restrain pathological adipose tissue remodeling and protect vascular integrity in obese mice. *EMBO reports* 22, e52835. <https://doi.org/10.15252/embr.202152835>
- Chi, J., Crane, A., Wu, Z., Cohen, P., 2018. Adipo-Clear: A Tissue Clearing Method for Three-Dimensional Imaging of Adipose Tissue. *J Vis Exp* 58271. <https://doi.org/10.3791/58271>
- Costa, E.C., Silva, D.N., Moreira, A.F., Correia, I.J., 2019. Optical clearing methods: An overview of the techniques used for the imaging of 3D spheroids. *Biotechnology and Bioengineering* 116, 2742–2763. <https://doi.org/10.1002/bit.27105>
- Costantini, I., Cicchi, R., Silvestri, L., Vanzi, F., Pavone, F.S., 2019. In-vivo and ex-vivo optical clearing methods for biological tissues: review. *Biomed. Opt. Express*, BOE 10, 5251–5267. <https://doi.org/10.1364/BOE.10.005251>
- Cotillard, A., Poitou, C., Torcivia, A., Bouillot, J.-L., Dietrich, A., Klöting, N., Grégoire, C., Lolmede, K., Blüher, M., Clément, K., 2014. Adipocyte Size Threshold Matters: Link with Risk of Type 2 Diabetes and Improved Insulin Resistance After Gastric Bypass. *The Journal of Clinical Endocrinology & Metabolism* 99, E1466–E1470. <https://doi.org/10.1210/jc.2014-1074>
- Frayn, K.N., 1993. Insulin resistance and lipid metabolism. *Current Opinion in Lipidology* 4, 197.
- Geng, J., Zhang, X., Prabhu, S., Shahoei, S.H., Nelson, E.R., Swanson, K.S., Anastasio, M.A., Smith, A.M., 2021. 3D microscopy and deep learning reveal the heterogeneity of crown-like structure microenvironments in intact adipose tissue. *Science Advances* 7, eabe2480. <https://doi.org/10.1126/sciadv.abe2480>
- Girousse, A., Gil-Ortega, M., Bourlier, V., Bergeaud, C., Sastourné-Arrey, Q., Moro, C., Barreau, C., Guissard, C., Vion, J., Arnaud, E., Pradère, J.-P., Juin, N., Casteilla, L., Sengenès, C., 2019. The Release of Adipose Stromal Cells from Subcutaneous Adipose Tissue Regulates Ectopic Intramuscular Adipocyte Deposition. *Cell Reports* 27, 323–333.e5. <https://doi.org/10.1016/j.celrep.2019.03.038>
- Gomariz, A., Helbling, P.M., Isringhausen, S., Suessbier, U., Becker, A., Boss, A., Nagasawa, T., Paul, G., Goksel, O., Székely, G., Stoma, S., Nørrelykke, S.F., Manz, M.G., Nombela-Arrieta, C., 2018. Quantitative spatial analysis of haematopoiesis-regulating stromal cells in the bone marrow microenvironment by 3D microscopy. *Nat Commun* 9, 2532. <https://doi.org/10.1038/s41467-018-04770-z>
- Graham, B.T., Moore, A.C., Burris, D.L., Price, C., 2017. Sliding enhances fluid and solute transport into buried articular cartilage contacts. *Osteoarthritis and Cartilage* 25, 2100–2107. <https://doi.org/10.1016/j.joca.2017.08.014>
- Greenspan, P., Mayer, E.P., Fowler, S.D., 1985. Nile red: a selective fluorescent stain for intracellular lipid droplets. *Journal of Cell Biology* 100, 965–973. <https://doi.org/10.1083/jcb.100.3.965>

- Hagberg, C.E., Li, Q., Kutschke, M., Bhowmick, D., Kiss, E., Shabalina, I.G., Harms, M.J., Shilkova, O., Kozina, V., Nedergaard, J., Boucher, J., Thorell, A., Spalding, K.L., 2018. Flow Cytometry of Mouse and Human Adipocytes for the Analysis of Browning and Cellular Heterogeneity. *Cell Reports* 24, 2746-2756.e5. <https://doi.org/10.1016/j.celrep.2018.08.006>
- Hajer, G.R., van Haeften, T.W., Visseren, F.L.J., 2008. Adipose tissue dysfunction in obesity, diabetes, and vascular diseases. *European Heart Journal* 29, 2959–2971. <https://doi.org/10.1093/eurheartj/ehn387>
- Horckmans, M., Bianchini, M., Santovito, D., Megens, R.T.A., Springael, J.-Y., Negri, I., Vacca, M., Eusanio, M.D., Moschetta, A., Weber, C., Duchene, J., Steffens, S., 2018. Pericardial Adipose Tissue Regulates Granulopoiesis, Fibrosis, and Cardiac Function After Myocardial Infarction. *Circulation*. <https://doi.org/10.1161/CIRCULATIONAHA.117.028833>
- Horckmans, M., Diaz Villamil, E., Bianchini, M., De Roeck, L., Communi, D., 2022. Central role of PD-L1 in cardioprotection resulting from P2Y4 nucleotide receptor loss. *Front. Immunol.* 13. <https://doi.org/10.3389/fimmu.2022.1006934>
- Hruby, A., Hu, F.B., 2015. The Epidemiology of Obesity: A Big Picture. *Pharmacoeconomics* 33, 673–689. <https://doi.org/10.1007/s40273-014-0243-x>
- Jing, W., Qingchen, H., Minyue, G. a. O., Xiaopan, Z.H.U., Zitong, C., Shaokang, W., Guiju, S.U.N., 2021. Preventive Effect of Forsythin from *Forsythia suspensa* Leaves on Obesity Induced by High-Fat Diet in Rats. *FOOD SCIENCE* 42, 85. <https://doi.org/10.7506/spkx1002-6630-20201216-198>
- Kredel, L.I., Siegmund, B., 2014. Adipose-Tissue and Intestinal Inflammation – Visceral Obesity and Creeping Fat. *Front. Immunol.* 5. <https://doi.org/10.3389/fimmu.2014.00462>
- Laforest, S., Labrecque, J., Michaud, A., Cianflone, K., Tchernof, A., 2015. Adipocyte size as a determinant of metabolic disease and adipose tissue dysfunction. *Critical Reviews in Clinical Laboratory Sciences* 52, 301–313. <https://doi.org/10.3109/10408363.2015.1041582>
- Lallemant, L., Lebreton, C., Garfa-Traoré, M., 2020. Comparison of different clearing and acquisition methods for 3D imaging of murine intestinal organoids. *J Biol Methods* 7, e141. <https://doi.org/10.14440/jbm.2020.334>
- Le Jan, D., Siliman Misha, M., Destrumelle, S., Terceve, O., Thorin, C., Larcher, T., Ledevin, M., Desfontis, J.-C., Betti, E., Mallem, Y., 2024. Omega-3 Fatty Acid and Vitamin D Supplementations Partially Reversed Metabolic Disorders and Restored Gut Microbiota in Obese Wistar Rats. *Biology (Basel)* 13, 1070. <https://doi.org/10.3390/biology13121070>
- LeMieux, M.J., Kalupahana, N.S., Scoggin, S., Moustaid-Moussa, N., 2015. Eicosapentaenoic Acid Reduces Adipocyte Hypertrophy and Inflammation in Diet-Induced Obese Mice in an Adiposity-Independent Manner^{1,2}. *The Journal of Nutrition* 145, 411–417. <https://doi.org/10.3945/jn.114.202952>
- Majka, S.M., Miller, H.L., Helm, K.M., Acosta, A.S., Childs, C.R., Kong, R., Klemm, D.J., 2014. Analysis and Isolation of Adipocytes by Flow Cytometry, in: *Methods in Enzymology*. Elsevier, pp. 281–296. <https://doi.org/10.1016/B978-0-12-411619-1.00015-X>
- Marcelin, G., Gautier, E.L., Clément, K., 2022. Adipose Tissue Fibrosis in Obesity: Etiology and Challenges. *Annual Review of Physiology* 84, 135–155. <https://doi.org/10.1146/annurev-physiol-060721-092930>
- Neugebauer, J., Raulien, N., Arndt, L., Akkermann, D., Hobusch, C., Lindhorst, A., Fröba, J., Gericke, M., 2024. The Impact of Resident Adipose Tissue Macrophages on Adipocyte Homeostasis and Dedifferentiation. *International Journal of Molecular Sciences* 25, 13019. <https://doi.org/10.3390/ijms252313019>
- Pan, C., Cai, R., Quacquarelli, F.P., Ghasemigharagoz, A., Loubopoulos, A., Matryba, P., Plesnila, N., Dichgans, M., Hellal, F., Ertürk, A., 2016. Shrinkage-mediated imaging of entire organs and organisms using uDISCO. *Nat Methods* 13, 859–867. <https://doi.org/10.1038/nmeth.3964>
- Ramírez, N.M., Toledo, R.C.L., Moreira, M.E.C., Martino, H.S.D., Benjamin, L. dos A., de Queiroz, J.H., Ribeiro, A.Q., Ribeiro, S.M.R., 2017. Anti-obesity effects of tea from *Mangifera indica* L.

- leaves of the Ubá variety in high-fat diet-induced obese rats. *Biomedicine & Pharmacotherapy* 91, 938–945. <https://doi.org/10.1016/j.biopha.2017.05.015>
- Ruiz-Ojeda, F.J., Méndez-Gutiérrez, A., Aguilera, C.M., Plaza-Díaz, J., 2019. Extracellular Matrix Remodeling of Adipose Tissue in Obesity and Metabolic Diseases. *International Journal of Molecular Sciences* 20, 4888. <https://doi.org/10.3390/ijms20194888>
- Ryu, Y., Kim, Y., Park, S.-J., Kim, S.R., Kim, H.-J., Ha, C.M., 2023. Comparison of Light-Sheet Fluorescence Microscopy and Fast-Confocal Microscopy for Three-Dimensional Imaging of Cleared Mouse Brain. *Methods and Protocols* 6, 108. <https://doi.org/10.3390/mps6060108>
- Schmitt, P., Mandonnet, E., Perdreau, A., Angelini, E.D., 2013. Effects of slice thickness and head rotation when measuring glioma sizes on MRI: in support of volume segmentation versus two largest diameters methods. *J Neurooncol* 112, 165–172. <https://doi.org/10.1007/s11060-013-1051-4>
- Singh, G., Krauthamer, M., Bjälme-Evans, M., 2022. Wegovy (Semaglutide): A New Weight Loss Drug for Chronic Weight Management. *Journal of Investigative Medicine* 70, 5–13. <https://doi.org/10.1136/jim-2021-001952>
- Sun, K., Kusminski, C.M., Scherer, P.E., 2011. Adipose tissue remodeling and obesity. *J Clin Invest* 121, 2094–2101. <https://doi.org/10.1172/JCI45887>
- Tchkonia, T., Thomou, T., Zhu, Y., Karagiannides, I., Pothoulakis, C., Jensen, M.D., Kirkland, J.L., 2013. Mechanisms and Metabolic Implications of Regional Differences among Fat Depots. *Cell Metabolism* 17, 644–656. <https://doi.org/10.1016/j.cmet.2013.03.008>
- Theobalt, N., Hofmann, I., Fiedler, S., Renner, S., Dhom, G., Feuchtinger, A., Walch, A., Angelis, M.H. de, Wolf, E., Wanke, R., Blutke, A., 2021. Unbiased analysis of obesity related, fat depot specific changes of adipocyte volumes and numbers using light sheet fluorescence microscopy. *PLOS ONE* 16, e0248594. <https://doi.org/10.1371/journal.pone.0248594>
- Tian, T., Yang, Z., Li, X., 2021. Tissue clearing technique: Recent progress and biomedical applications. *Journal of Anatomy* 238, 489–507. <https://doi.org/10.1111/joa.13309>
- Wang, X., Xu, M., Li, Y., 2022. Adipose Tissue Aging and Metabolic Disorder, and the Impact of Nutritional Interventions. *Nutrients* 14, 3134. <https://doi.org/10.3390/nu14153134>
- Xiao, Y., Liu, D., Cline, M.A., Gilbert, E.R., 2020. Chronic stress and adipose tissue in the anorexic state: endocrine and epigenetic mechanisms. *Adipocyte* 9, 472–483. <https://doi.org/10.1080/21623945.2020.1803643>

FIGURES

Figure 1. Methodological Workflow for 3D Imaging and Analysis of Mesenteric Adipose Tissue.

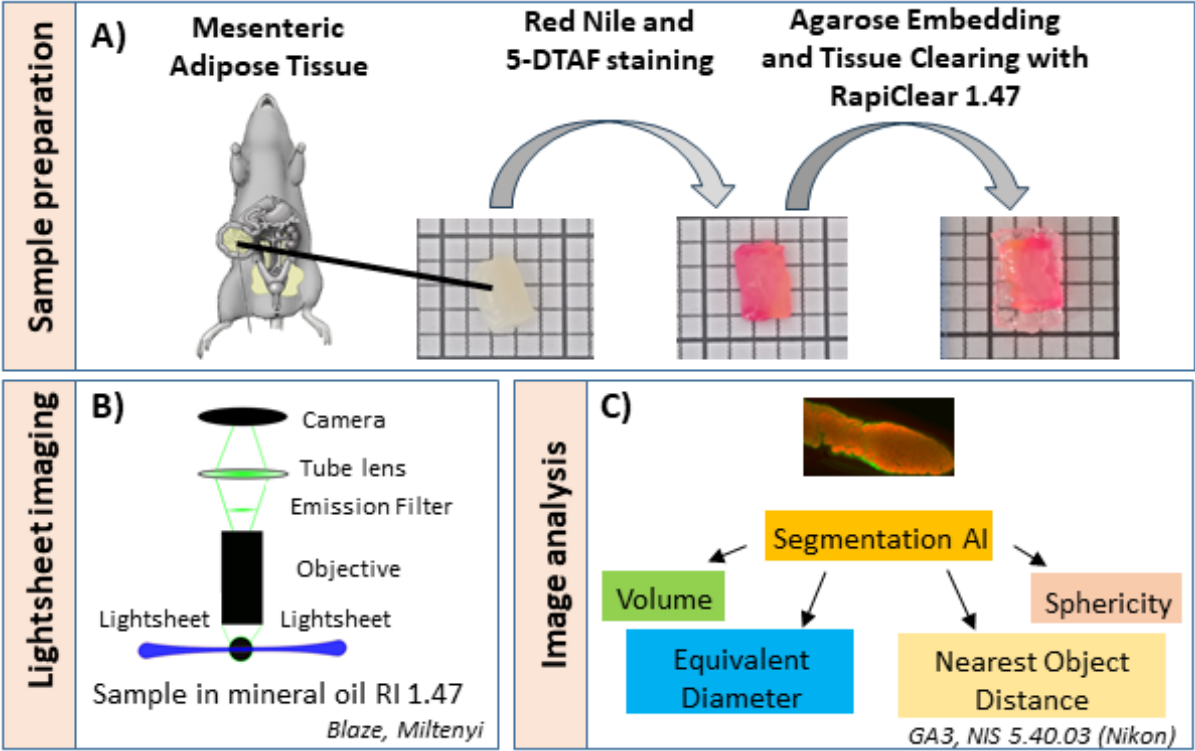


Figure 2. Deep Learning-Based Adipocyte Segmentation and 3D Image Analysis Pipeline.

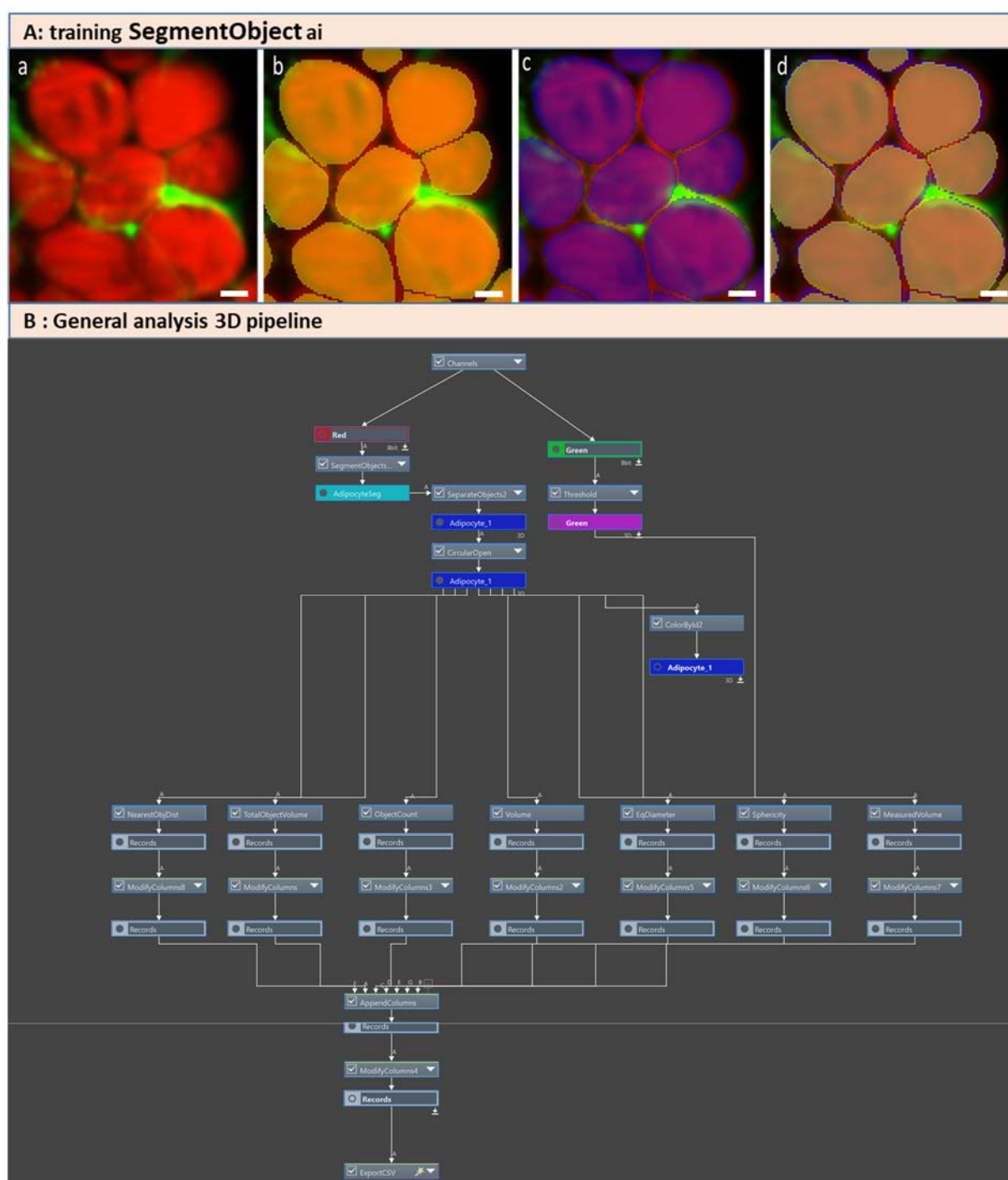


Figure 3. 3D Visualization and Segmentation of Cleared Adipose Tissue in Healthy and Obese Groups.

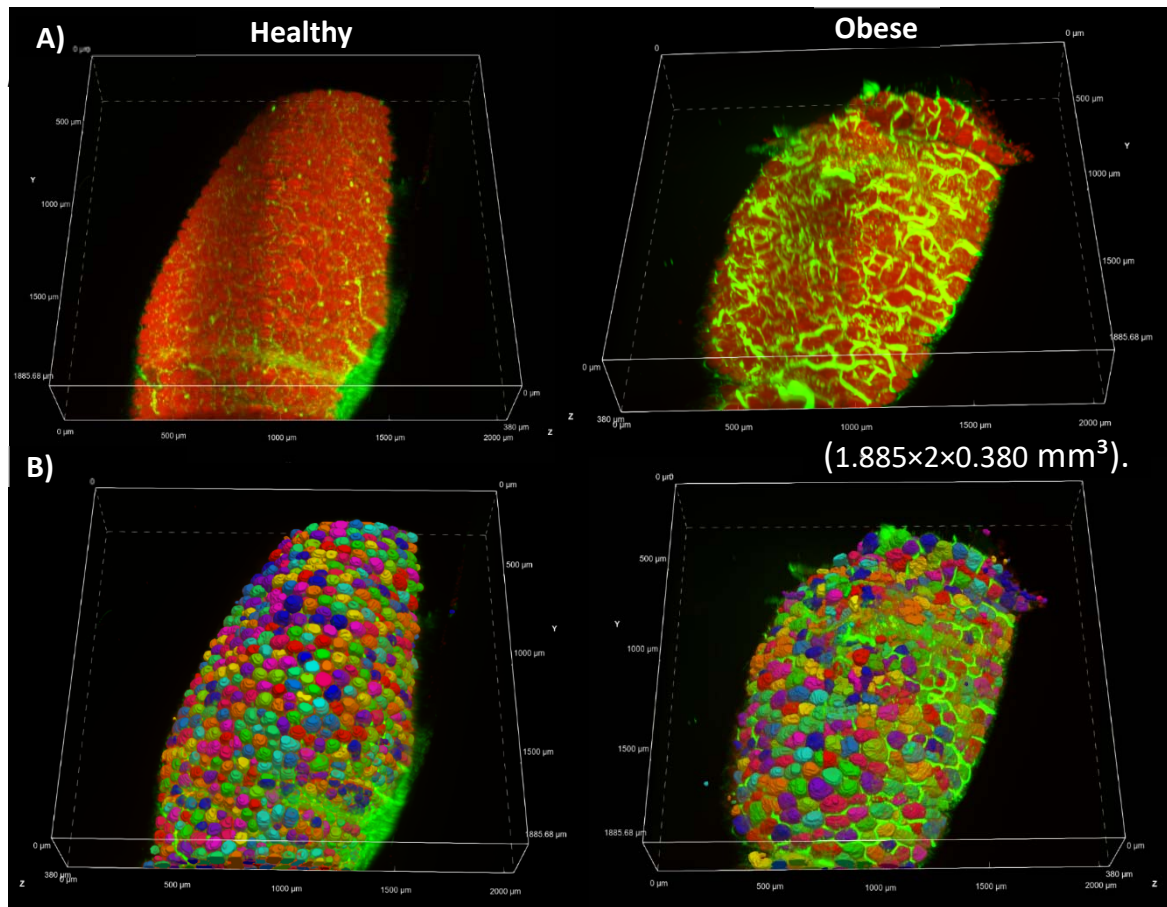
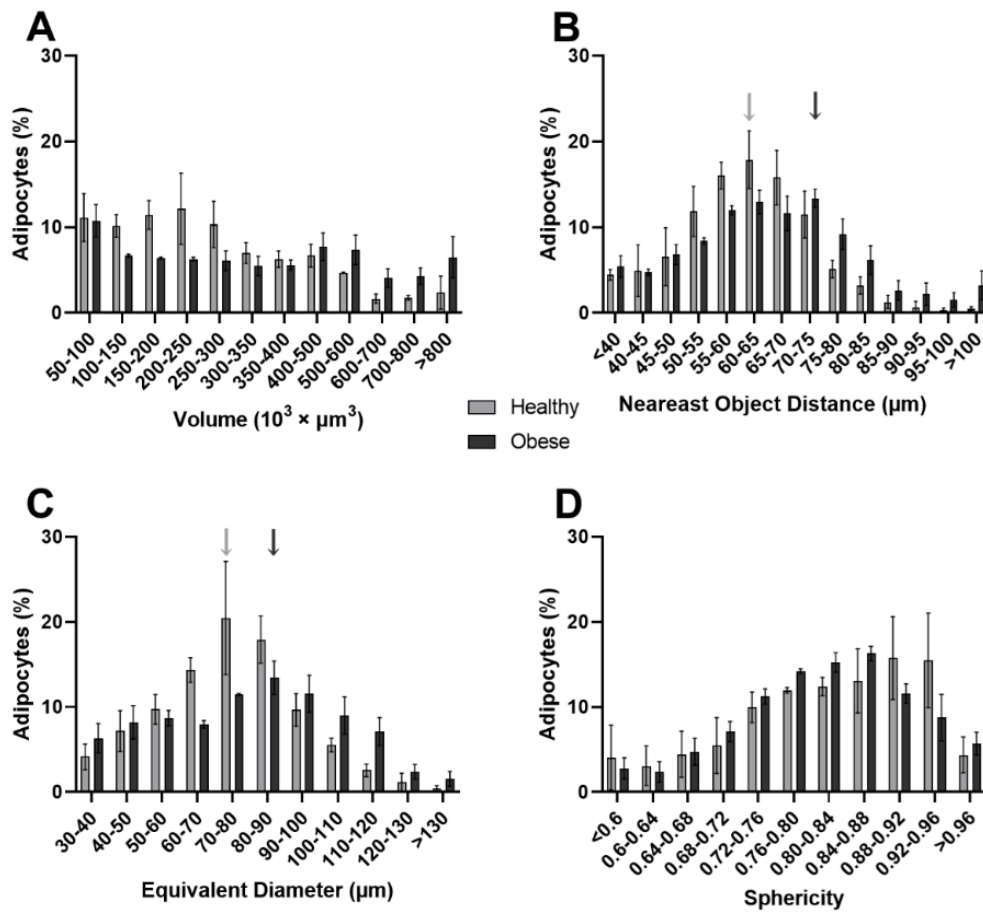


Figure 5. Distribution of adipocyte characteristics in the Healthy and Obese groups.



FIGURES LEGENDS

Figure 1. Methodological Workflow for 3D Imaging and Analysis of Mesenteric Adipose Tissue.

A) Sample Preparation: Tissue is extracted from rat mesenteric adipose depots, stained with Red Nile and 5-DTAF, embedded in agarose, and cleared using RapiClear 1.47. B) LightSheet Imaging: Cleared samples are imaged using a LightSheet fluorescence microscope (Blaze, Miltenyi) with a 4X objective and mineral oil immersion (RI 1.47). C) Image Analysis: Segmentation AI processes the acquired images to extract key adipocyte morphological parameters, including volume, equivalent diameter, nearest object distance, and sphericity, using GA3 and NIS 5.40.03 software (Nikon).

Figure 2 Deep Learning-Based Adipocyte Segmentation and 3D Image Analysis Pipeline. A: Application of the algorithm SegmentObject.ai generated from training, the cropped images highlight the efficiency of the predictions generated by the deep learning models for adipocyte segmentation: **a**: Cropped image with adipocyte labelled with Nile red (red) and extracellular matrix labelled with 5-DTAF (green). **b**: Cropped image annotated using the initial version of the algorithm, followed by manual correction. **c**: Cropped image processed with the updated algorithm after training the deep learning model. **d**: Overlay of the segmentations produced by the initial and updated algorithms, demonstrating their alignment and differences. Scale bar = 25 μm . Learning model was also evaluated from Loss curve (training Loss 0.00279 with 1500 iterations). B: General Analysis 3 pipeline (NIS-Elements software version 5.42.03, Nikon Europe B.V.) for 3D image analyses including resulting segmentobject.ai algorithm to measure total object volume, object count, individual object volume, equivalent diameter, sphericity, and nearest object distance (NOD).

Figure 3. 3D Visualization and Segmentation of Cleared Adipose Tissue in Healthy and Obese Groups. A: 3D visualization of RapiClear 1.47 cleared adipose tissue stained with Nile red (adipocytes in red) and 5-DTAF (extracellular matrix in green) in Healthy and Obese groups. Observation with LightSheet ultramicroscope Blaze, objective 4X ($1.885 \times 2 \times 0.380 \text{ mm}^3$). B: segmented 3D adipocytes using the SegmentObject.ai module in NIS-Elements software (version 5.42.03, Nikon Europe BV, Amstelveen).

Figure 4. Evaluation of adipocyte characteristics in the Healthy and Obese groups: (A) Adipocyte volume (μm^3), (B) Nearest object distance (NOD, μm) between adipocytes, (C) Adipocyte equivalent diameter (μm), and (D) Adipocyte sphericity. Quantification was done using a fully automated image processing algorithm using NIS-Elements software. All results are expressed as mean \pm standard error of the mean, with $n=1647$ adipocytes. Statistical significance was determined using Mann-Whitney tests. ***: $p\text{-value} < 0.001$; ns: non-significant.

Figure 5. Distribution of adipocyte characteristics in the Healthy and Obese groups: (A) Adipocyte volume (μm^3), (B) Nearest Object Distance (NOD, μm), (C) Adipocyte Equivalent Diameter (μm), and (D) Adipocyte sphericity. Arrows indicate the location of the maximal peak (light for Healthy and dark for Obese) for NOD and Equivalent Diameter. All results are expressed as the mean number of adipocytes in each class with $n=3$ rats. Statistical significance was determined using multiple Mann-Whitney tests; however, no significant differences were observed between the groups.